AGU PUBLICATIONS

Geophysical Research Letters

RESEARCH LETTER
10.1002/2015GL064485

Key Points:
- Earth OH($\Delta v = 1, 2$) emissions are studied simultaneously with VIRTIS/Rosetta
- Relative OH population values for v = 1 to 9 are derived from measurements
- Comparison with previous observations and models are provided

Correspondence to:
A. Migliorini,
Alessandra.Migliorini@iaps.inaf.it

Citation:
Migliorini, A., J. C. Gérard, L. Soret, G. Piccioni, F. Capaccioni, G. Filacchione, M. Snels, and F. Tosi (2015), Terrestrial OH nightglow measurements during the Rosetta flyby, *Geophys. Res. Lett.*, *42*, doi:10.1002/2015GL064485.

Received 7 MAY 2015
Accepted 22 JUN 2015
Accepted article online 26 JUN 2015

Terrestrial OH nightglow measurements during the Rosetta flyby

A. Migliorini[1], J. C. Gérard[2], L. Soret[2], G. Piccioni[1], F. Capaccioni[1], G. Filacchione[1], M. Snels[3], and F. Tosi[1]

[1]INAF-Istituto di Astrofisica e Planetologia Spaziali, Rome, Italy, [2]LPAP, Université de Liège, Liège, Belgium, [3]ISAC-CNR, Rome, Italy

Abstract We present a study of the terrestrial hydroxyl nightglow emissions observed with the Visible and Infrared Thermal Imaging Spectrometer on board the Rosetta mission. During these observations, the OH $\Delta v = 1$ and 2 sequences were measured simultaneously. This allowed investigating the relative population of the $v = 1$ to 9 vibrational levels by using both sequences. In particular, the relative population of the vibrational level $v = 1$ is determined for the first time from observations. The vibrational population decreases with increasing vibrational quantum number. A good agreement is found with a recent model calculation assuming multiquantum relaxation for OH(v) quenching by O_2 and single-quantum relaxation for OH(v) by N_2.

1. Introduction

The Meinel bands of hydroxyl are a good proxy to investigate atmospheric properties on the terrestrial planets. These emissions have been extensively used to study the photochemical and dynamical properties of the Earth's upper mesosphere. Vibrationally excited OH is produced through the Bates-Nicolet mechanism following the chemical reaction [*Bates and Nicolet*, 1950]:

$$H + O_3 \rightarrow OH*(v \leq 9) + O_2 \quad (1)$$

which is effective in the Earth, Mars, and Venus atmospheres. The reaction involving HO_2 short-lived molecules

$$O + HO_2 \rightarrow OH*(v \leq 6) + O_2 \quad (2)$$

was found to be negligible for the excitation of the Earth's OH Meinel bands with v up to 6 [*Meriwether*, 1989], although its role is still debated, as discussed in *Xu et al*. [2012].

On Earth, the OH airglow layer is located near the mesopause [*Lowe et al*., 1996; *She and Lowe*, 1998], with a maximum at 87 km and a full width at half maximum (FWHM) of about 8 km [*Baker and Stair*, 1988].

Several studies based on ground- and space-based observations demonstrated that the OH Meinel emission profile is strongly sensitive to the atmospheric temperature and density profiles. Dynamic structures, like tides [*Xu et al*., 2010; *Zhang et al*., 1998; *Shepherd et al*., 1998; *Ward*, 1999; *Zhang and Shepherd*, 1999; *Russell et al*., 2005; *Liu et al*., 2008] or planetary waves [*Snively et al*., 2010; *Gao et al*., 2010], are found to affect the peak altitude by modulating the OH emission profile. Quenching by atomic oxygen also contributes to the vertical shift observed in the peak altitudes from different Meinel bands [*von Savigny and Lednyts'kyy*, 2013]. Temperature inversions and minor species mixing effects are also responsible for changes in the OH airglow vertical profile [*Melo et al*., 1999; *von Savigny et al*., 2012]. Moreover, it has been observed that the emission originating from higher vibrational levels typically occurs at higher altitudes [*von Savigny et al*., 2012]. Spectroscopy of the OH airglow has also been used to infer the mesospheric temperature at the airglow altitudes [*Zhao et al*., 2005; *She and Lowe*, 1998].

Here we present an analysis of the OH($\Delta v = 1, 2$) sequences in the Earth's atmosphere, observed with the Visible and Infrared Thermal Imaging Spectrometer (VIRTIS) on board the Rosetta spacecraft, during the Earth flyby in November 2009, in order to obtain the population distribution of the vibrational levels.

The observing geometry has limited the lowest accessible altitude to 87 km, with a vertical resolution on the order of 10 km/pixel at best. Hence, we limit our investigation to the altitude range 87–105 km, without exploring the vertical dependence of the emission. Moreover, the spectral resolution is not adequate to resolve single rovibrational transitions, and the vibrational manifolds are only partly resolved. For this reason, we assume that a Gaussian shape reproduces the emission layer.

Our analysis will be compared with previous ground-based and space observations and with model calculations. The method we employ in this analysis offers the advantage of being less sensitive to spurious signals and instrumental artifacts because it uses the $\Delta v = 1$ and $\Delta v = 2$ spectra which were simultaneously observed. In addition, spectra observed from space are not affected by telluric absorptions; hence, the full OH($\Delta v = 1$, 2) sequences of emissions can be retrieved without correction for atmospheric extinction.

In section 2 the analysis of the VIRTIS/Rosetta spectral data is described, focusing on the terrestrial OH nightglow emission in the infrared. An empirical radiative model of the spectral range where OH($\Delta v = 1$, 2) emissions occur is described in section 3 with the aim to allow a retrieval of the vibrational populations. In section 4, we discuss the results and compare them with analyses of experimental ground-based observations and theoretical works.

2. Data Selection

Rosetta is the first large-class European mission devoted to the close investigation of small bodies in the Solar System [*Schulz*, 2009]. It was launched on 2 March 2004 toward the primary target of the mission, comet 67P/Churyumov-Gerasimenko (67P/C-G). The main scientific objectives of the Rosetta mission dealt with the study of the comet 67P/C-G, with special emphasis on its nucleus and coma. Gravity assist maneuvers with the Earth and Mars [*Coradini et al*., 2010; *Migliorini et al*., 2013] were performed during the 10 year long cruise phase, as well as flybys with the main belt asteroids (2867) Steins [*Tosi et al*., 2010; *Leyrat et al*., 2011] and (21) Lutetia [*Coradini et al*., 2011]. The investigation of the planetary airglow emissions is one of the goals foreseen for the mission during the Earth and Mars flybys.

The VIRTIS instrument [*Coradini et al*., 2007] includes two spectral channels: (1) the VIRTIS-M mapping spectrometer, with imaging capabilities and a medium spectral resolution and (2) the VIRTIS-H echelle spectrometer, with a higher spectral resolution compared to VIRTIS-M but without imaging capabilities. VIRTIS-M covers the 0.3–5.1 μm range in 864 spectral bands by means of two coaligned channels: the visible/near-infrared channel, operating from 0.3 to 1.0 μm with a spectral sampling of 2 nm; and the IR channel, from 1.0 to 5.1 μm with a spectral sampling of 9.5 nm; the spectral resolution is of the order of 3 nm and 20 nm in the visible and infrared, respectively. Each data cube in the visible and/or infrared has a dimension of $432 \times N_s \times N_l$, where 432 is the number of spectral channels, N_l (number of lines) depends on the length of the observation, while N_s (number of samples) is the number of spatial pixels composing a line, usually equal to 256. The field of view of each square-shaped pixel is 0.25 mrad wide; hence, a 256 pixel × 256 pixel image, obtained by using a scanning mirror, covers a 64 mrad × 64 mrad field (which corresponds to 220 arc min × 220 arc min). The full field of view (FOV) is acquired in time by repeating successive acquisitions, while the internal steerable mirror performs a scan or maintaining it at fixed position while the spacecraft is drifting (pushbroom mode). The Earth data discussed here were acquired in the scan mode, allowing one to acquire a sequence of limbs consecutively.

The two VIRTIS-M focal planes are equipped with order-sorting filters to reduce contaminations due to higher spectral orders coming from the diffraction gratings. The two filters placed on the visible channel's detector have a junction placed at 0.640–0.651 μm; the five on the infrared channel detector have four junctions corresponding to 1.415–1.576 μm, 2.388–2.548 μm, 3.671–3.765 μm, and 4.284–4.397 μm wavelength [*Coradini et al*., 2007]. In general, the spectral radiance measured through the junctions has been corrected by the calibration pipeline. However, despite this correction some residual signals remain present on the first two junctions of the IR channel.

Since VIRTIS-M spectral range extends up to 5.1 μm, thermal environment plays a major role in the instrumental performance. During the flyby, the VIRTIS radiator FOV was partially filled with the Earth, resulting in an optical bench temperature of about 147 K, significantly larger than the typical operative temperature of 135 K. This excess in temperature results in a wavelength shift of ~11 nm in the spectral calibration [*Migliorini et al*., 2013], which was corrected in the calibration pipeline [*Filacchione et al*., 2006].

In this paper we focus our analysis on data acquired in the IR spectral range, during the Earth gravity assist that occurred in November 2009. Prior to this flyby, two more gravity assists with our planet had been performed by Rosetta on 4 March 2005 and between 13 and 14 November 2007. They will not be discussed

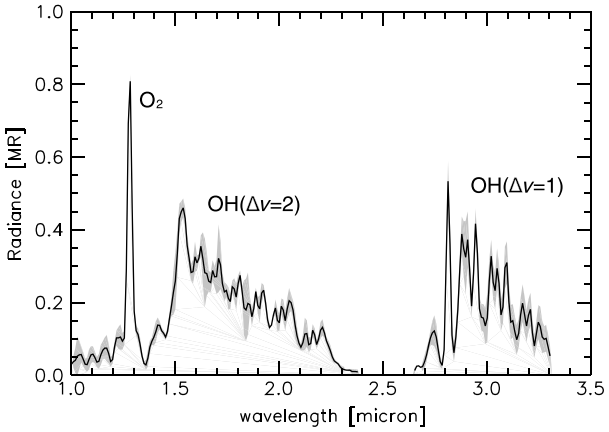

Figure 1. VIRTIS mean nightglow spectral radiance, in the altitude range 87–105 km. This data set was processed with a median filter applied to the spatial component, in order to eliminate instrumental artifacts and with a background correction obtained by subtracting the spectrum measured between 120 and 125 km. Finally, a spectral calibration adjustment has been performed by applying a shift of ~11 nm toward shorter wavelengths (see also *Migliorini et al.* [2013]). The shaded area indicates the experimental error, calculated from the Noise Equivalent Spectral Radiance. The O_2 and OH($\Delta v = 1, 2$) emissions are indicated.

here because the observations were not suitable to study nightglow emissions. During the first flyby, no limb observation was performed, while during the second flyby the limb mode observations concentrated on the dayside.

In the approach phase of the November 2009 Rosetta Earth flyby, a sequence of full-disk images of the nightside of the planet was acquired by VIRTIS-M from a distance spanning the range 228,000–240,000 km. These data were not suitable for the O_2 and OH nightglow investigation because of the low spatial resolution and hence are not considered in this study. When the spacecraft was less than 55,000 km away from the Earth, limb scans of the night side were carried out, starting from 150 km above the surface. These data satisfy our requirements to study the nightglow emission; the resulting vertical resolution (13–15 km/pixel) is similar to the thickness of the emission layer, and the duration of each scan (2 min) is short enough to minimize possible time variability of the emissions.

The VIRTIS airglow data (image name I1_00216713355) consist of a collection of two limb scans in the same image, acquired a few minutes apart. The total duration of the IR channel scan is 12 min, corresponding to a sequence of 73 lines with an integration time of 7 s each. The two limbs cover the latitude region from 38° to 47° in the Northern Hemisphere and are centered at 1:30–2:00 A.M. solar local time. A more detailed description of the Earth's observations with VIRTIS was given in *Migliorini et al.* [2013] and *Hurley et al.* [2014].

In order to remove high-frequency spatial noise, the cube image was cleaned using a median filter combined with a smoothing procedure, applied in the spatial direction while the temporal and spectral dimensions were kept unchanged.

Since it was verified that the emission is roughly located at about 90 km, we averaged a total of 300 radiance spectra collected between 87 and 105 km in order to increase the signal-to-noise ratio. The analysis was applied to the two VIRTIS observations separately, because the contribution of the background is different from one scan to the other. The radiance was converted into Rayleigh (R) units, where $1\,R = 10^6$ photons/$cm^2\,s^{-1}$ in 4π steradians. The resulting spectrum is shown in Figure 1 for one of the two limb scans.

In the mean spectrum, the O_2 emission centered at 1.27 μm is clearly observed, as well as the $\Delta v = 2$ OH Meinel bands in the 1.4–2.4 μm region, and $\Delta v = 1$ band in the 2.7–3.3 μm region, as indicated in Figure 1. The spectral region beyond 3.5 μm is dominated by the thermal emission and will not be discussed here.

Due to the limited spectral and spatial resolution, the variation of the peak emission's altitude occurring for the different transitions as studied by several authors [*Kaufmann et al.*, 2008; *McDade*, 1991; *von Savigny et al.*, 2012; *von Savigny and Lednyts'kyy*, 2013] cannot be verified in VIRTIS data set.

3. Spectral Model

We use the PGOPHER code (http://pgopher.chm.bris.ac.uk) to generate the line intensities of the rotational transitions for each vibrational band. The population distribution of the rotational levels is assumed to be Maxwellian. A rotational temperature of 200 K has been used in order to calculate a synthetic spectrum of the OH($\Delta v = 1$ and 2) emissions. This temperature is close to the average value at the mesopause [*Xu et al.*, 2012]. The variation of the rotational temperature with the vibrational levels has been discussed

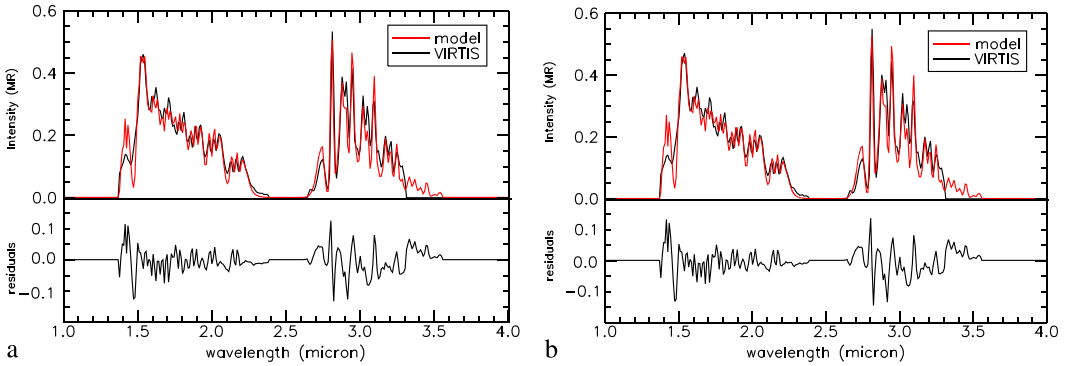

Figure 2. (a) Comparison between the VIRTIS spectrum (in black) and the spectral model (in red) for the first limb scan. The radiance outside the wavelengths regions covered by the OH emissions is set to 0, to limit the fit to the spectral region involving OH emissions. The residuals are shown in Figure 2a (bottom). (b) The same for the second limb scan.

in *Cosby and Slanger* [2007] and *Noll et al.* [2014]. The difference between the rotational temperature in the $v = 1$ manifold with respect to the $v = 10$ manifold may be as large as 20 K. We simulated the rotational manifold for three different temperatures (200 K, 250 K, and 300 K) and compared the simulations, convolved to the VIRTIS spectral resolution of 20 nm, with the observed spectra. It appeared that a rotational temperature of 200 K produced the best agreement. We note, however, that a rotational temperature difference of the order of 15–20 K only affects the structure inside each band, whose effect is negligible at the VIRTIS resolution. The emission spectra of the OH Meinel bands can thus be simulated by multiplying the calculated rotational manifolds for all vibrational quantum numbers ($v = 1$–9) with the (unknown) populations of the upper levels and the relative Einstein coefficients for each vibrational transition. The Einstein coefficients were taken from *Xu et al.* [2012], calculated for a temperature of 200 K. The variation of the Einstein coefficients with temperature is very small [see, e.g., *Xu et al.*, 2012], and thus, our simulation is largely independent of the rotational temperature assumed. We then performed a least squares fit, which yielded the relative populations of the vibrational levels ($v = 1$ to 9), taking into account both $\Delta v = 1$ and $\Delta v = 2$ bands. Figures 2a and 2b shows the comparison between the VIRTIS spectra and the corresponding best fit for the available data.

Similarly, a fit is obtained for the second VIRTIS spectrum, acquired within a few minutes from the first one. Both fits are in good agreement and provide consistent results for the populations of levels from $v = 1$ to 9, except for the region between 1.4 and 1.5 μm, where a VIRTIS order-sorting filter junction is located. The model overestimates the intensity of the (2–0) transition at 1.46 μm in both spectra. The same discrepancy was observed by comparing the Thermosphere, Ionosphere, Mesosphere, Energetics, and Dynamics (TIMED)/Sounding of the Atmosphere Using Broadband Emission Radiometry (SABER) observations with models, as reported by *Xu et al.* [2012]. The TIMED/SABER observations had been corrected for the atmospheric attenuation, mostly due by water vapor. The good agreement between the fit and VIRTIS observations of the (2–1) transition (around 2.82 μm) seems to exclude a specific quenching of the $v = 2$ level. A possible explanation for this effect may be an error in the Einstein coefficient.

The average values of each population obtained for the two fits are provided in Table 1. To calculate the error in the vibrational populations, a set of 40 spectra was statistically generated by adding a random error to the original spectra. Each spectrum so obtained was fitted in the same way as the VIRTIS spectra, and the standard deviation of the results was taken as errors in the determination of the vibrational population. Values of the percentage into each v level for the two spectra, together with the calculated statistical error, are shown in Table 1.

4. Discussion

The terrestrial nightglow emissions at the midlatitudes of the Northern Hemisphere have been investigated by using VIRTIS observations during a Rosetta Earth flyby. During the season (November) of these observations, the OH nightglow is quite intense at the altitudes, local time, and latitudes observed by VIRTIS, as reported also by the Wind Imaging Interferometer [*Liu et al.*, 2008].

Table 1. The Fitted OH Vibrational Population From the Two VIRTIS Spectra[a]

Level	Population—First Fit	Error	Population—Second Fit	Error
1	37.8	1.0	37.58	1.03
2	21.02	1.15	20.33	1.19
3	17.95	0.8	18.36	0.83
4	7.27	0.46	7.40	0.48
5	4.88	0.30	4.92	0.31
6	3.59	0.26	3.66	0.27
7	2.91	0.21	2.99	0.22
8	2.77	0.20	2.84	0.20
9	1.83	0.24	1.91	0.25

[a]The population values are given in terms of percentage, together with the associated absolute errors (in percentages).

The vibrationally excited hydroxyl radical can decay through spontaneous emission of a photon, giving rise to the observed emission, or can be quenched through collisions with other ambient molecules (N_2 and O_2) or atoms (O). The quenching process can occur stepwise involving transitions from a specific vibrational level to a lower vibrational level, or all at once to the vibrational ground level. This so-called sudden death mechanism, which can occur by vibrational quenching or by chemical reaction, results in a smaller population of the low vibrational levels. While the radiative processes merely depend on the Einstein coefficients, which are rather independent of temperature, the quenching processes depend on the reaction rates, which may have a strong temperature dependence and on the availability of quenchers. This implies that the vibrational population of the OH radical also may depend on the time and latitude of the observation.

We compare our results with ground-based measurements reported in *Krassovsky et al*. [1962], *Ferguson and Parkinson* [1963], *Harrison and Kendall* [1973], *Turnbull and Lowe* [1983], and *Oliva and Origlia* [1992].

The heterogeneity of the previous measurements reported in the literature limits the comparison to a few vibrational levels, which are present in all the considered data sets. For this reason, the comparison is made by normalizing all relative populations to that of the $v=4$ level, which has been reported by all authors. In the considered previous works [*Krassovsky et al*., 1962; *Ferguson and Parkinson*, 1963; *Harrison and Kendall*, 1973; *Turnbull and Lowe*, 1983], authors provided values directly comparable with the vibrational populations retrieved on VIRTIS data. *Oliva and Origlia* [1992], on the other hand, provided a list of resolved rotational lines of hydroxyl, from which we derived the vibrational populations, by summing the identified lines for each level. As stated also by the authors, the band list is sometimes incomplete or limited by experimental issues, such as the atmospheric attenuation, so that the calculated populations have to be considered as lower limits.

VIRTIS data were also compared with model calculations by *Llewellyn et al*. [1978], *von Clarmann et al*. [2010], and *Xu et al*. [2012]. The model proposed by *von Clarmann et al*. [2010] produces excited OH in all vibrational levels ($v=1$–10), by the hydrogen-ozone reaction. They used the Generic RAdiative traNsfer AnD non-LTE population Algorithm model [*Funke et al*., 2012] to calculate the relative OH populations for vibrational levels 0 to 9, for six different atmospheric conditions, assuming a stepwise quenching by O_2, N_2, and O. The model case describing a "midlatitudes night" atmosphere is the only one close to the observing conditions of the VIRTIS data discussed here. Hence, in Table 2 we report von Clarmann's results only for this model conditions. Note that the rate coefficients for OH production and for the quenching processes were much different from those used by *Llewellyn et al*. [1978]. *Xu et al*. [2012] compared the TIMED/SABER observations at 1.6 and 2.0 μm, including four OH transitions of the $\Delta v=2$ sequence, with a nightglow emission model. They concluded that reaction (a) is the dominant source for the OH nightglow emission for the vibrational levels with $v\geq 4$. The assumption of multiquantum relaxation by O_2 and single-quantum relaxation by N_2 produced the best agreement with the SABER data, while the sudden death model could not reproduce the observations.

Except for our high $v=3$ population, all the relative populations from *Krassovsky et al*. [1962]; *Harrison and Kendall* [1973], and *Ferguson and Parkinson* [1963] are in reasonable agreement with those derived here. We examined the possibility that the order-sorting filter at 1.415–1.576 μm could cause some residual instrumental effect [see, e.g., *Tosi et al*., 2012], but repeating the fits without this spectral interval did not produce appreciable changes in the results.

The studies of *Krassovsky et al*. [1962] and *Harrison and Kendall* [1973] were based on observations of the $\Delta v=3$, 4, 5, 6 and the $\Delta v=2$, 3, 4, 5 sequences, but no information about the $v=1$ level could be obtained. Our analysis yields a population for the $v=1$ level which is about 5 times higher than the $v=4$ level. None

Table 2. Comparison of Relative Vibrational Populations With Previous Studies[a]

	This work	*Krassovsky et al.* [1962][b]	*Ferguson and Parkinson* [1963][b]	*Harrison and Kendall* [1973][b]	*Turnbull and Lowe* [1983][b]	*Oliva and Origlia* [1992][b]	*Llewellyn et al.* [1978][c]	*von Clarmann et al.* [2010][c]	*Xu et al.* [2012][c]
	38–47°N	55–62°N	55–62°N	56°N	43°N	29°S	45°N	Midlatitudes	30–50°N
Level	Nov 2009	1957–1958	1957–1958	Dec 1971	Apr 1980	Apr 1991			
1	5.1 ± 0.5						4.16	3.27	4.47
2	2.8 ± 0.36				2.83	0.47	2.24	1.85	2.41
3	2.47 ± 0.29	1.73	1.96	1.27	1.76	1.44	1.43	1.31	1.50
4	1.00 ± 0.14	1.00	1.00	1.00	1.00	1.00	1.00	1.00	1.00
5	0.67 ± 0.09	0.67	0.80	0.57		0.77	0.78	0.77	0.68
6	0.49 ± 0.07	0.40	0.47	0.44	0.25	0.26	0.60	0.59	0.47
7	0.40 ± 0.06	0.29	0.38	0.27	0.17	0.01	0.52	0.49	0.35
8	0.38 ± 0.05	0.23	0.24	0.29	0.16	0.26	0.52	0.33	0.30
9	0.25 ± 0.05	0.18	0.22	0.17	0.16	0.22	0.51	0.19	0.22

[a]Values are normalized at $v = 4$, for which all considered works provide values.
[b]Ground-based observations.
[c]Numerical model.

of the previous analyses of experimental observations allowed the determination of the population of the $v = 1$ level, while only two of them report the population of $v = 2$. Of these two, the value of *Turnbull and Lowe* [1983] is very similar to ours, while those reported by *Oliva and Origlia* [1992] seem unrealistic. The population of $v = 1$ level has been calculated by using different model simulations. *Llewellyn et al.* [1978] calculated a ratio of 4.16 for the $v = 1$ population relative to the $v = 4$ population, while *Xu et al.* [2012] reported a ratio of 4.47, which is in reasonable agreement with the one obtained from the VIRTIS data. The value by *von Clarmann et al.* [2010] is significantly lower (3.27). The populations of levels 1 to 3 are underestimated in *von Clarmann et al.* [2010], while those with $v > 4$ are higher than the populations derived from the VIRTIS/Rosetta data. These discrepancies and the difference with the populations calculated by *Xu et al.* [2012] possibly stem from the use of a single-quantum relaxation in collisions with O by von Clarmann et al., whereas other models assume sudden death chemical loss, where the excited OH molecule is directly deactivated to the $v = 0$ ground level. Another difference lies in the treatment of collisions with O_2 as von Clarmann et al. assume single-quantum relaxation, while Xu et al. adopt a multiquantum scheme.

Bunn and Gush [1972] also measured the $\Delta v = 1$, 2 sequences using balloon-borne instruments. They found relative populations to be $P(v = 1)/P(v = 2) = 2.26$ and $P(v = 2)/P(v = 3) = 1.76$. Our study suggests ratios of 1.82 (16) and 1.13(12), respectively. The populations calculated from the intensities of sky emissions taken from *Oliva and Origlia* [1992] do not follow the trend of decreasing populations with increasing levels. It appears that their $v = 2$ and $v = 7$ populations are largely underestimated. In fact, these authors mention that some of the band intensities could be underestimated by large factors as they lie in regions of low atmospheric transmission.

Observations with the same VIRTIS instrument on the European Venus Express mission allowed discovering the OH infrared night airglow on the Venus nightside in 2007 [*Piccioni et al.*, 2008]. The OH airglow spectra on the two planets show some differences in the intensity distribution of the different bands. For example, the relative intensities of the $\Delta v = 1$ bands originating from $v' > 2$ levels are higher in the terrestrial spectrum than in the Venus case. This difference is presumably linked to the much larger abundance of CO_2 in the Venus atmosphere. On Venus (and presumably on Mars), CO_2 is the dominant quencher, while O_2 and O play the major role on Earth to deactivate vibrationally excited OH. *Soret et al.* [2012] demonstrated that for Venus, compared with these terrestrial results, the paradigm of single vibrational quantum collision deactivation by CO_2 provides a much better agreement with both the spectral structure and the observed total brightness than the "sudden death" model.

5. Conclusions

For the first time, the data analyzed in this study allow investigating the OH infrared nightglow emission from space and the vibrational population down to $v = 1$. The $\Delta v = 1$ and $\Delta v = 2$ sequences have been observed simultaneously. We remind, however, that VIRTIS spatial and spectral resolution does not allow a complete retrieval of the vertical profile of each single transition and hence our measurements are limited. No

correction for the telluric absorption is needed, and the populations deduced for the 1 to 9 vibrational levels might thus be considered as quite reliable.

The results of our analysis have been compared with ground-based observations and theoretical models. A rather good agreement is found with the model proposed by *Xu et al.* [2012], which assumed multiquantum relaxation by O_2 and single-quantum relaxation by N_2. The slightly smaller populations for the levels $v = 1–3$ in *Xu et al.* [2012] can possibly be explained by the omission of reaction (b) in their calculation.

Acknowledgments
The authors wish to thank ESA, ASI, and the national space agencies supporting the Rosetta mission (grant: ASI-INAF I/024/12/0). L. Soret and J.-C. Gérard are supported by the PRODEX program managed by ESA with the help of the Belgian Federal Space Science Policy Office. The authors thank Xu and von Clarmann for kindly providing numerical values from their previous works.

The Editor thanks Christian von Savignyand an anonymous reviewer for their assistance in evaluating this paper.

References

Baker, D. J., and A. T. Stair Jr. (1988), Rocket measurements of the altitude distributions of the hydroxyl airglow, *Phys. Scr.*, *37*, 611–622, doi:10.1088/0031-8949/37/4/021.

Bates, D. R., and M. Nicolet (1950), The photochemistry of atmospheric water vapor, *J. Geophys. Res.*, *55*, 301–327, doi:10.1029/JZ055i003p00301.

Bunn, F. E., and H. P. Gush (1972), Spectrum of the airglow between 3 and 4 microns, *Can. J. Phys.*, *50*, 213–215, doi:10.1139/p72-033.

Coradini, A., et al. (2007), Virtis: An imaging spectrometer for the Rosetta mission, *Space Sci. Rev.*, *128*, 529–559, doi:10.1007/s11214-006-9127-5.

Coradini, A., et al. (2010), Martian atmosphere as observed by VIRTIS-M on Rosetta spacecraft, *J. Geophys. Res.*, *115*, E04004, doi:10.1029/2009JE003345.

Coradini, A., et al. (2011), The surface composition and temperature of Asteroid 21 Lutetia as observed by Rosetta/VIRTIS, *Science*, *334*, 492–494, doi:10.1126/science.1204062.

Cosby, P. C., and T. G. Slanger (2007), OH spectroscopy and chemistry investigated with astronomical sky spectra, *Can. J. Phys.*, *85*, 77–99.

Ferguson, A. F., and D. Parkinson (1963), The hydroxyl bands in the nightglow, *Planet. Space Sci.*, *11*, 149–159, doi:10.1016/0032-0633(63)90136-3.

Filacchione, G., et al. (2006), On-ground characterization of Rosetta/VIRTIS-M. II. Spatial and radiometric calibrations, *Rev. Sci. Instrum.*, *77*, 103–106.

Funke, B., M. López-Puertas, M. García-Comas, M. Kaufmann, M. Höpfner, and G. P. Stiller (2012), GRANADA: A Generic RAdiative transfer AnD non-LTE population algorithm, *J. Quant. Spectrosc. Radiat. Transfer*, *113*(14), 1771–1817.

Gao, H., J. Xu, and Q. Wu (2010), Seasonal and QBO variations in the OH nightglow emission observed by TIMED/SABER, *J. Geophys. Res.*, *115*, A06313, doi:10.1029/JA014641.

Harrison, A. W., and D. J. W. Kendall (1973), Airglow hydroxyl intensity measurements 0.6–2.3 μm, *Planet. Space Sci.*, *21*, 1731–1741, doi:10.1016/0032-0633(73)90164-5.

Hurley, J., P. G. J. Irwin, A. Adriani, M. Moriconi, F. Oliva, F. Capaccioni, A. Smith, G. Filacchione, F. Tosi, and G. Thomas (2014), Analysis of Rosetta/VIRTIS spectra of earth using observations from ENVISAT/AATSR, TERRA/MODIS and ENVISAT/SCIAMACHY, and radiative-transfer simulations, *Planet. Space Sci.*, *90*, 37–59, doi:10.1016/j.pss.2013.06.012.

Kaufmann, M., C. Lehmann, L. Hoffmann, B. Funke, M. López-Puertas, C. V. Savigny, and M. Riese (2008), Chemical heating rates derived from SCIAMACHY vibrationally excited OH limb emission spectra, *Adv. Space Res.*, *41*, 1914–1920, doi:10.1016/j.asr.2007.07.045.

Krassovsky, V. I., N. N. Shefov, and V. I. Yarin (1962), Atlas of the airglow spectrum 3000–12400 Å, *Planet. Space Sci.*, *9*(12), 883–915, doi:10.1016/0032-0633(62)90008-9.

Leyrat, C., A. Coradini, E. Erard, F. Capaccioni, M. T. Capria, P. Drossart, M. C. De Sanctis, F. Tosi, and the Rosetta/VIRTIS Team (2011), Thermal properties of the asteroid (2867) Steins as observed by VIRTIS/Rosetta, *Astron. Astrophys.*, *531*(A168), doi:10.1051/0004-6361:201116529.

Liu, G., G. G. Shepherd, and R. G. Roble (2008), Seasonal variations of the nighttime O(1S) and OH airglow emission rates at mid-to-high latitudes in the context of the large-scale circulation, *J. Geophys. Res.*, *113*, A06302, doi:10.1029/2007JA012854.

Llewellyn, E. J., B. H. Long, and B. H. Solheim (1978), The quenching of OH* in the atmosphere, *Planet. Space Sci.*, *26*, 525–531, doi:10.1016/0032-0633(78)90043-0.

Lowe, R. P., L. M. Leblanc, and K. L. Gilbert (1996), WINDII/UARS observation of twilight behavior of the hydroxyl airglow, at mid-latitude equinox, *J. Atmos. Sol. Terr. Phys.*, *58*, 1863–1896, doi:10.1016/0021-9169(95)00178-6.

McDade, I. C. (1991), The altitude dependence of the OH($X^2\Pi$) vibrational distribution in the nightglow: Some model expectations, *Planet. Space Sci.*, *39*, 1049–1057, doi:10.1016/0032-0633(91)90112-N.

Melo, S. M. L., R. P. Lowe, and H. Takahashi (1999), The nocturnal behaviour of the hydroxyl airglow at the equatorial and low latitudes as observed by WINDII: Comparison with ground-based measurements, *J. Geophys. Res.*, *104*, 24,657–24,665, doi:10.1029/1999JA900291.

Meriwether, J. W. (1989), A review of the photochemistry of selected nightglow emissions from the mesopause, *J. Geophys. Res.*, *94*, 14,629–14,646, doi:10.1029/JD094iD12p14629.

Migliorini, A., et al. (2013), Comparative analysis of airglow emissions in terrestrial planets, observed with VIRTIS-M instruments on board Rosetta and Venus Express, *Icarus*, *226*, 1115–1127, doi:10.1016/j.icarus.2013.07.027.

Noll, S., et al. (2014), OH populations and temperatures from 25 bands, *Atmos. Chem. Phys. Discuss.*, *14*, 32,979–33,043.

Oliva, E., and L. Origlia (1992), The OH airglow spectrum: A calibration source for infrared spectrometers, *Astron. Astrophys.*, *254*, 466–471.

Piccioni, G., et al. (2008), First detection of hydroxyl in the atmosphere of Venus, *Astron. Astrophys.*, *483*, L29–L33, doi:10.1051/0004-6361:200809761.

Russell, J. P., W. E. Ward, R. P. Lowe, R. G. Roble, G. G. Shepherd, and B. Solheim (2005), Atomic oxygen profiles (80 to 115 km) derived from wind imaging interferometer/upper atmospheric research satellite measurements of the hydroxyl and green line airglow: Local time-altitude dependence, *J. Geophys. Res.*, *110*, D15305, doi:10.1029/2004JD005570.

Schulz, R. (2009), Rosetta—One comet rendezvous and two asteroids fly-bys, *Solar Syst. Res.*, *43*, 343–352, doi:10.1134/S0038094609040091.

She, C. Y., and R. P. Lowe (1998), Seasonal temperature variations in the mesospause region at mid-latitude: Comparison of lidar and hydroxyl rotational temperatures using WINDII/UARS heights profiles, *J. Atmos. Sol. Terr. Phys.*, *60*, 1573–1583, doi:10.1016/S1364-6826(98)00082-0.

Shepherd, G. G., R. Roble, S. P. Zhang, C. McLandress, and R. Wiens (1998), Tidal influence on midlatitude airglow: Comparison of satellite and ground-based observations with TIME-GCM predictions, *J. Geophys. Res.*, *103*, 14,741–14,751, doi:10.1029/98JA00884.

Snively, J. B., V. P. Pasko, and M. J. Taylor (2010), OH and OI airglow layer modulation by ducted short-period gravity waves: Effects of trapping altitude, *J. Geophys. Res.*, *115*, A11311, doi:10.1029/2009JA015236.

Soret, L., J. C. Gérard, G. Piccioni, and P. Drossart (2012), The OH Venus nightglow spectrum: Intensity and vibrational composition from VIRTIS-Venus Express observations, *Icarus*, *73*, 387–396, doi:10.1016/j.pss.2012.07.027.

Tosi, F., et al. (2010), The light curve of Asteroid 2867 Steins measured by VIRTIS-M during the Rosetta fly-by, *Planet. Space Sci.*, *58*, 1066–1076, doi:10.1016/j.pss.2010.03.019.

Tosi, F., et al. (2012), The light curve of Asteroid 21 Lutetia measured by VIRTIS-M during the Rosetta fly-by, *Planet. Space Sci.*, *66*, 9–22, doi:10.1016/j.pss.2011.11.016.

Turnbull, D. N., and R. P. Lowe (1983), Vibrational population distribution in the hydroxyl night airglow, *Can. J. Phys.*, *61*, 244–250, doi:10.1139/p83-033.

von Clarmann, T., et al. (2010), Do vibrationally excited OH molecules affect middle and upper atmospheric chemistry?, *Atmos. Chem. Phys.*, *10*, 9953–9964, doi:10.5194/acp-10-9953-2010.

von Savigny, C., and O. Lednyts'kyy (2013), On the relationship between atomic oxygen and vertical shifts between OH Meinel bands originating from different vibrational levels, *Geophys. Res. Lett.*, *40*, 5821–5825, doi:10.1002/2013GL058017.

von Savigny, C., I. C. McDade, K. U. Eichmann, and J. P. Burrows (2012), On the dependence of the OH Meinel emission altitude on vibrational level: SCIAMACHY observations and model simulations, *Atmos. Chem. Phys.*, *12*, 8813–8828, doi:10.5194/acp-12-8813-2012.

Ward, W. E. (1999), A simple model of diurnal variations in the mesospheric oxygen nightglow, *Geophys. Res. Lett.*, *26*, 3565–3568, doi:10.1029/1999GL003661.

Xu, J., A. K. Smith, G. Jiang, H. Gao, Y. Wei, and M. G. Mlynczak (2010), Strong longitudinal variations in the OH nightglow, *Geophys. Res. Lett.*, *37*, L21801, doi:10.1029/2010GL043972.

Xu, J., H. Gao, A. K. Smith, and Y. Zhu (2012), Using TIMED/SABER nightglow observations to investigate hydroxyl emission mechanisms in the mesopause region, *J. Geophys. Res.*, *117*, D02301, doi:10.1029/2011JD016342.

Zhang, S. P., and G. G. Shepherd (1999), The influence of the diurnal tide on the O(^{1}S) and OH emission rates observed by WINDII on UARS, *Geophys. Res. Lett.*, *26*, 529–532, doi:10.1029/1999GL900033.

Zhang, S. P., R. Wiens, B. Solheim, and G. Shepherd (1998), Nightglow zenith emission rate variations in the O(^{1}S) at low latitudes from wind imaging interferometer (WINDII), *J. Geophys. Res.*, *103*, 6251–6259, doi:10.1029/97JD03326.

Zhao, Y., M. J. Taylor, and X. Chu (2005), Comparison of simultaneous Na lidar and mesospheric nightglow temperature measurements and the effects of tides on the emission layer heights, *J. Geophys. Res.*, *110*, D09S07, doi:10.1029/2004JD005115.